Electronic Supplementary Material (ESI) for Journal of Materials Chemistry A.

Supporting Information

Surface energy-driven *ex-situ* hierarchical assembly of low-dimensional nanomaterials on graphene aerogels: A versatile strategy

Long Pan,‡[a,*] Peiyuan Gao,‡[b] Elena Tervoort,[a] Alexandre M. Tartakovsky[b] and Markus Niederberger[a,*]

[a] Laboratory for Multifunctional Materials, Department of Materials, ETH Zurich, Vladimir-Prelog-Weg 5, 8093, Zurich, Switzerland

[b] Advanced Computing, Mathematics, and Data Division, Pacific Northwest National Laboratory, Richland, Washington, 99352, United States

Email: long.pan@mat.ethz.ch, markus.niederberger@mat.ethz.ch

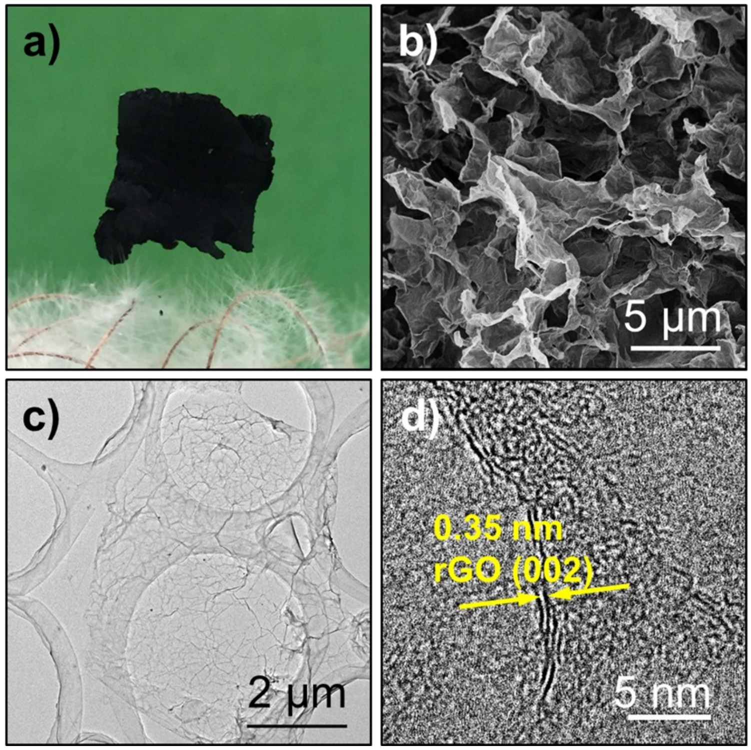

Figure S1. (a) Photograph, and (b) SEM, (c) TEM and (d) HRTEM images of the freestanding rGO aerogel. As seen in panel (a), the rGO aerogel can be supported by an ultralight Clematis Virgin's Bower seed, indicating the extremely low density of the aerogel.

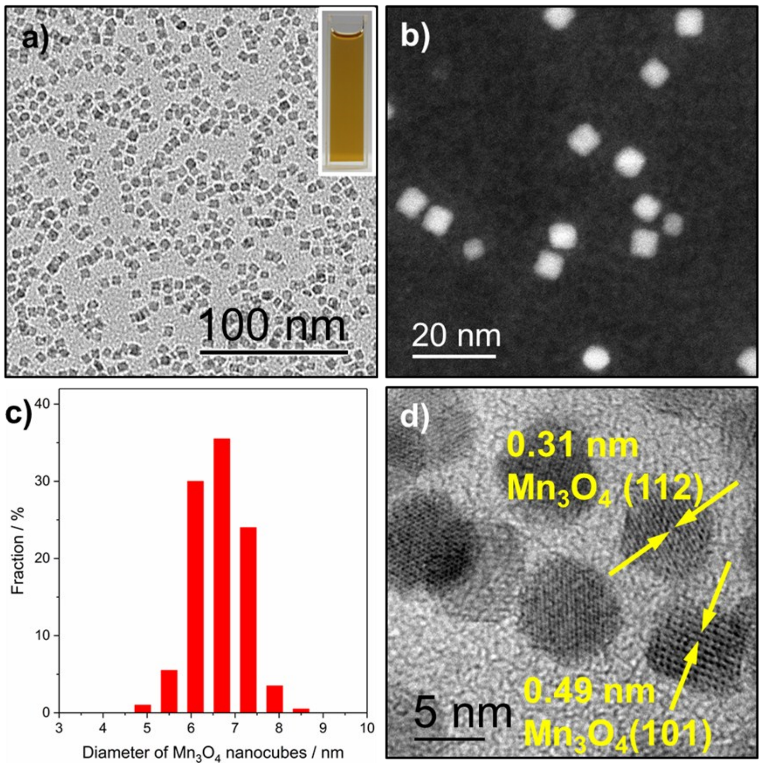

Figure S2. (a) TEM and (b) STEM images, (c) histogram of diameter-distribution, and (d) HRTEM image of Mn_3O_4 nanocubes. The inset in (a) is a photograph of a Mn_3O_4/THF dispersion. TEM and STEM show that the Mn_3O_4 are monodisperse nanocubes with an average diameter of 6.5 nm (200 nanoparticles are counted). HRTEM image displays the tetragonal Mn_3O_4 (hausmannite) nanocubes with distinct lattice spacings of 0.31 and 0.49 nm corresponding to the (112) and (101) planes.[S1] It should be pointed out that the Mn_3O_4 nanocubes can be stably dispersed in THF and hexane for months without any, if few, precipitate, indicating the low surface energy of Mn_3O_4 nanocubes in THF and hexane.

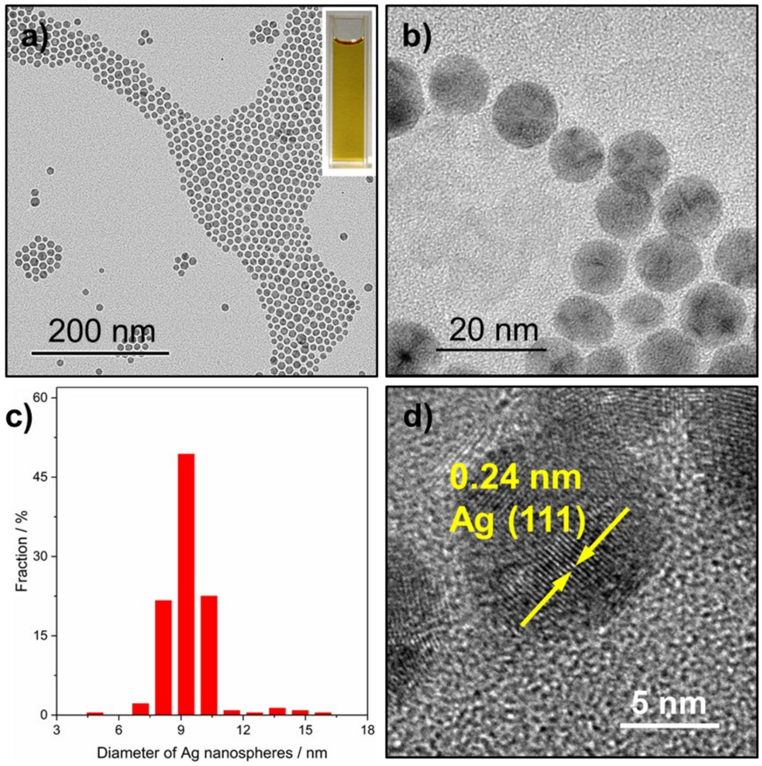

Figure S3. (a) Low- and (b) high-magnification TEM images, (c) histogram of diameter-distribution, and (d) HRTEM images of Ag nanospheres. The inset in (a) is a photograph of an Ag/THF dispersion. Ag nanospheres are monodisperse nanoparticles with an average diameter of 9.3 nm (200 nanoparticles are counted). A well-defined lattice spacing of 0.24 nm attributed to the (111) plane of face-centered cubic Ag can be apparently identified in HRTEM.[S2] The Ag nanospheres are energetically stable at THF for months (inset in (a)), implying its low surface energy.

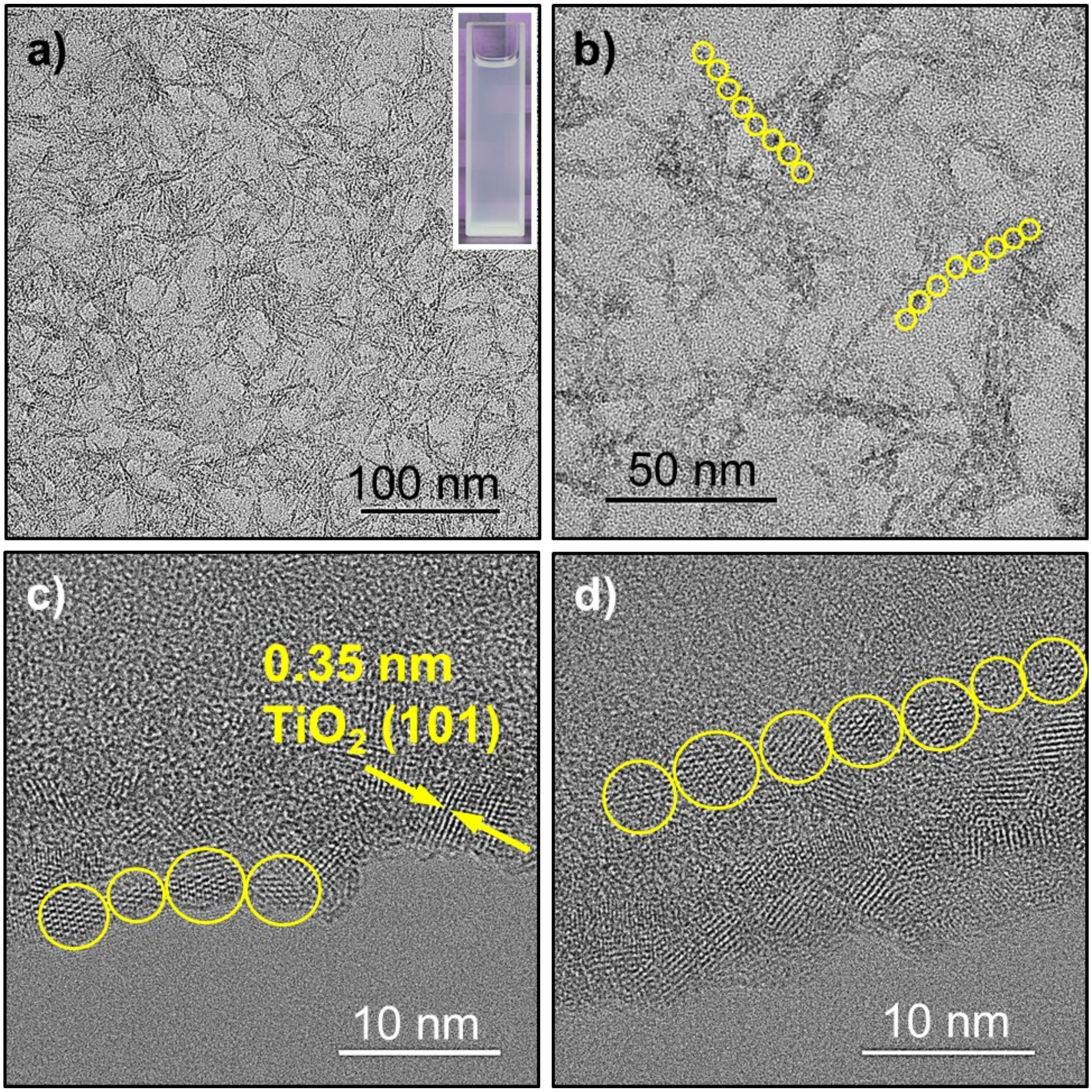

Figure S4. (a) Low- and (b) high-magnification TEM, and (c) and (d) HRTEM images of TiO_2 nanochains. The inset in (a) is a photograph of a TiO_2/methanol dispersion. The TiO_2 nanochains are composed of small TiO_2 nanoparticles (diameter = ca. 3 nm) attaching to each other with the (001) facets,[S3] which are illustrated by the yellow circles in TEM and HRTEM. The lattice spacing of 0.35 nm can be assigned to the (101) plane of anatase TiO_2.[S3]

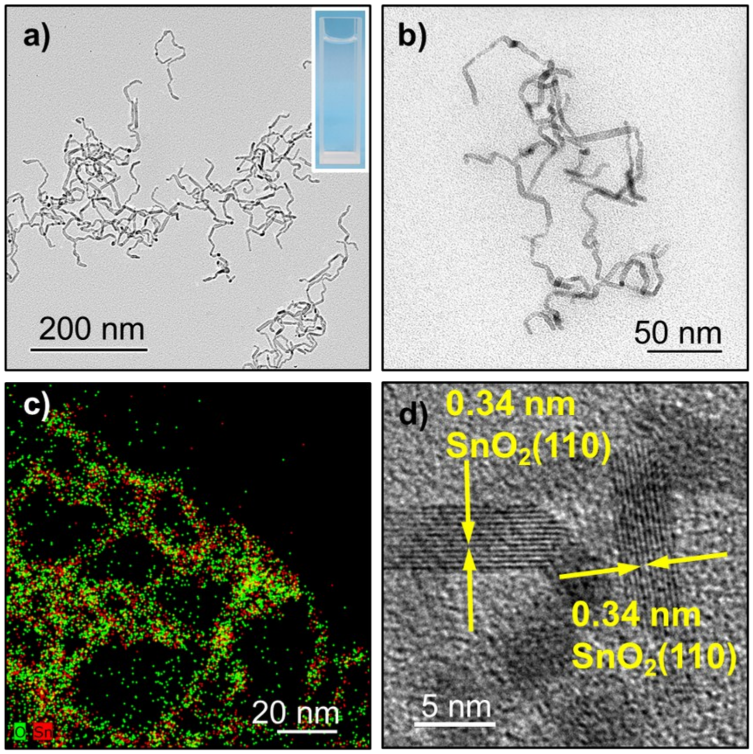

Figure S5. (a) Low- and (b) high-magnification TEM images, (c) STEM image with element mappings, and (d) HRTEM image of SnO_2 nanowires. The SnO_2 nanowires are almost monodisperse with an average length of ca. 200 nm and diameter of ca. 4.5 nm. The element mappings show that the distributions of Sn and O are in good agreement with the morphology of SnO_2, demonstrating that the nanowires are composed of SnO_2. The HRTEM image further confirms the rutile phase of SnO_2.[S4] The SnO_2/THF dispersion can be stable for months, implying the low surface energy of SnO_2 nanowires in THF.

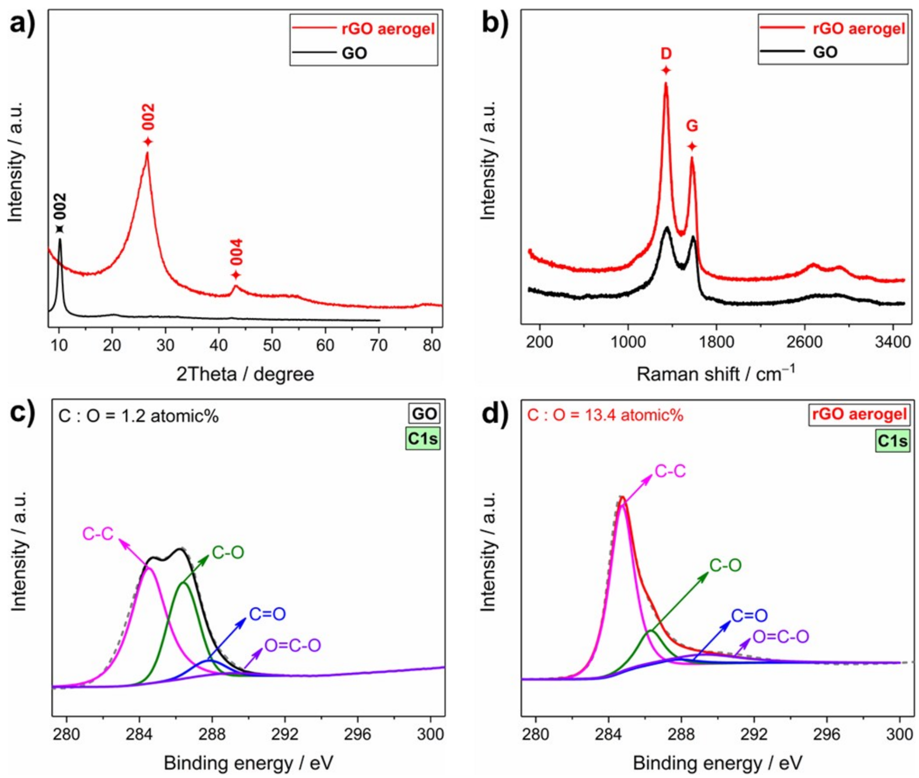

Figure S6. (a) XRD patterns and (b) Raman spectra of GO and rGO aerogels; C 1s XPS spectra of (c) GO and (d) rGO aerogels. The interlayer spacing decreases from 0.87 nm of GO to 0.34 nm, pointing to reduction of GO to rGO. Besides, the intensity ratio of the D and G bands (I_D/I_G) in Raman is indicative for the degree of defects in carbon materials. Obviously, the value of I_D/I_G in rGO aerogels (1.51) is higher than that of GO (1.14), evidencing that GO is successfully reduced to rGO. The result is in good agreement with that reported by others.[S5–S7] The reason for this observation is a decreased average size of the sp^2-hybridized domains upon reduction of GO, and thus an increased quantity of new graphitic domains with smaller sizes. As seen from the XPS spectra, obviously the C/O atomic ratio increases dramatically from 1.2 in GO to 13.4 in rGO aerogels, once again demonstrating that GO has been successfully reduced to rGO.

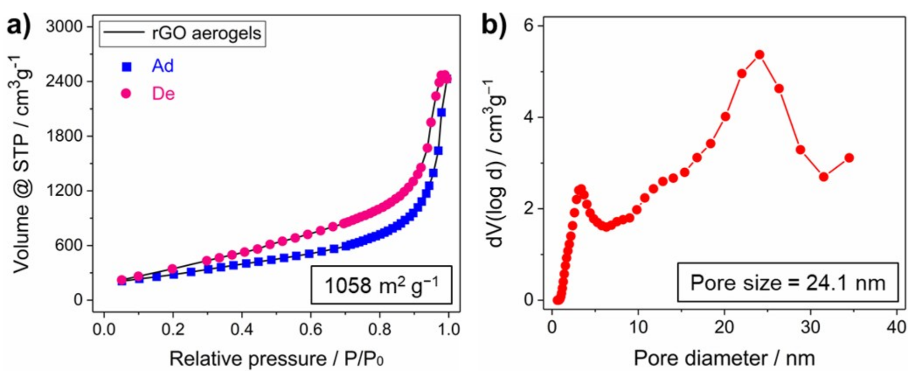

Figure S7. (a) N_2 adsorption-desorption isotherms and (b) pore size distribution of rGO aerogels.

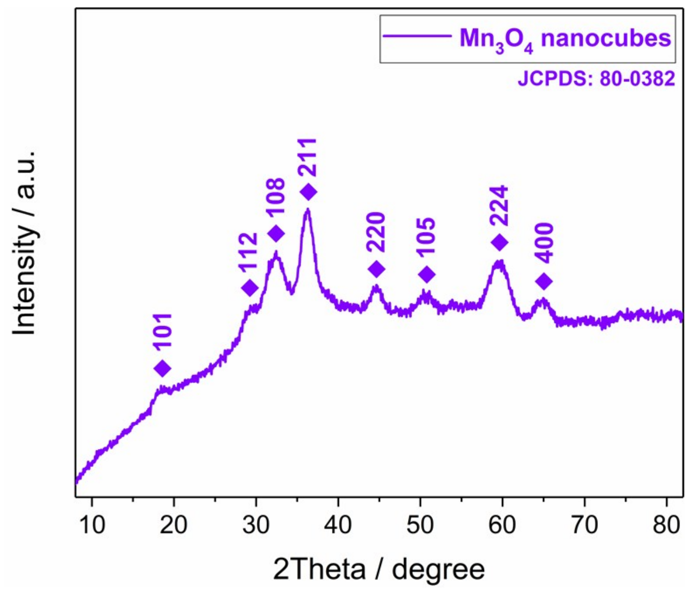

Figure S8. XRD pattern of Mn_3O_4 nanocubes.

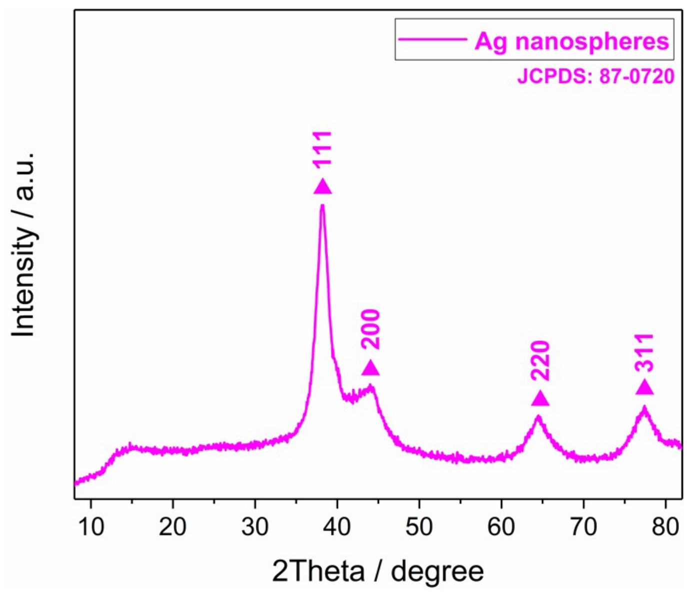

Figure S9. XRD pattern of Ag nanospheres.

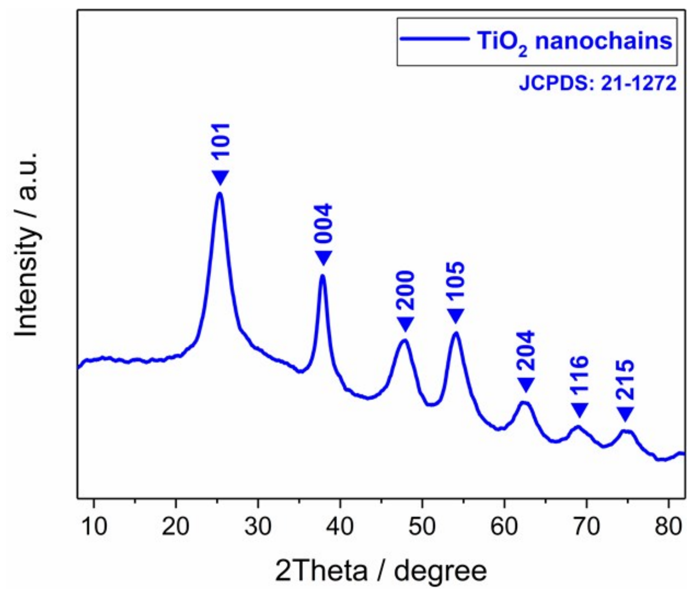

Figure S10. XRD pattern of TiO_2 nanochains.

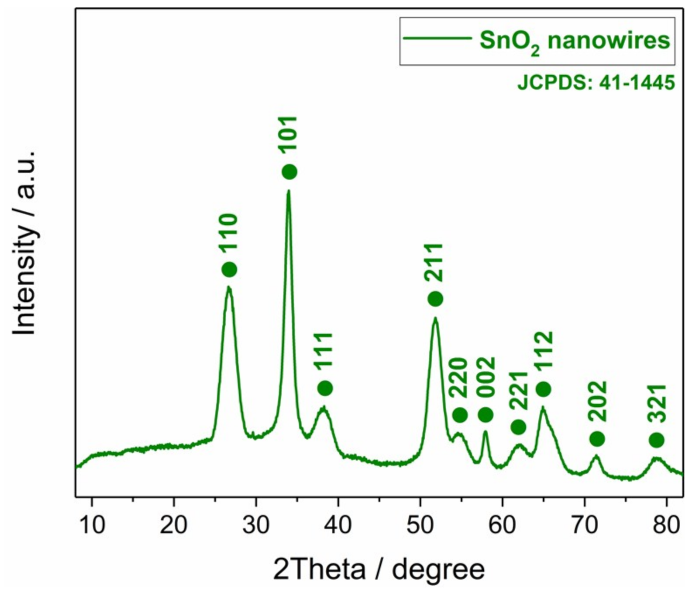

Figure S11. XRD pattern of SnO_2 nanowires.

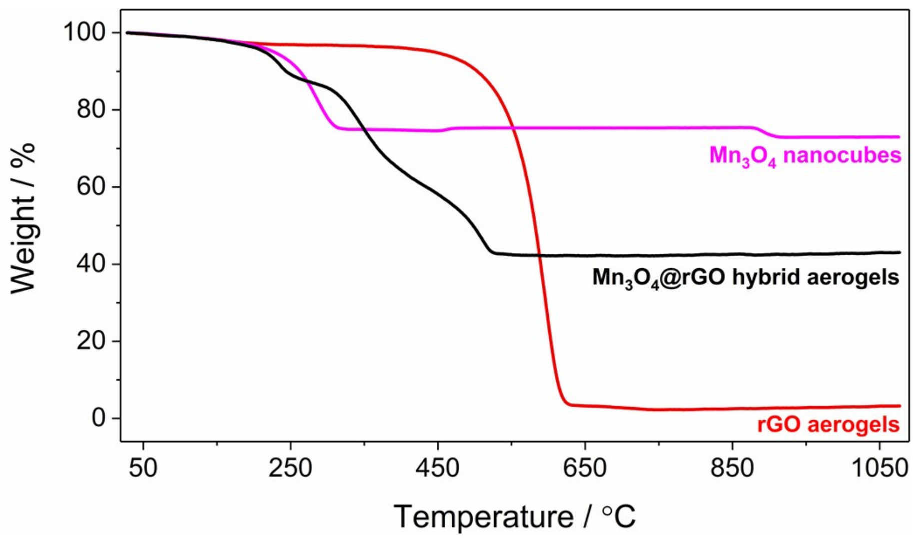

Figure S12. TGA curves of Mn_3O_4 nanocubes, rGO aerogels and Mn_3O_4@rGO hybrid aerogels.

Table S1. Weight ratio of Mn_3O_4 nanocubes and rGO aerogels in the Mn_3O_4@rGO hybrid aerogels.

	Mn_3O_4 nanocubes	rGO aerogels
Actual ratio	58 wt%	42 wt%
Feed ratio	60 wt%	40 wt%

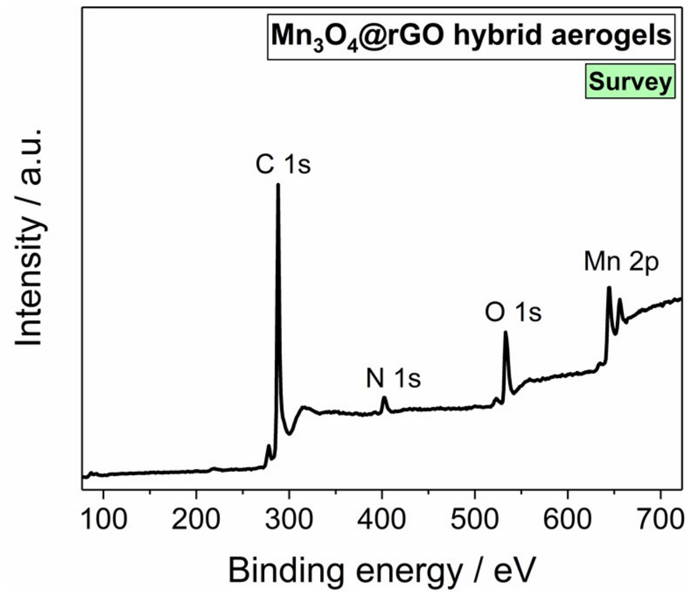

Figure S13. XPS survey spectrum of Mn_3O_4@rGO hybrid aerogels. The small peak assigned to N originates from ethylenediamine (EDA), which is in good agreement with other reports.[S5]

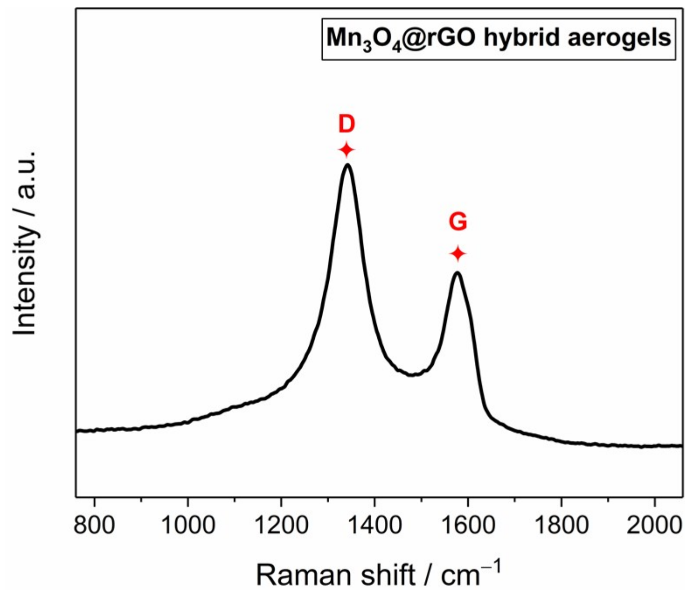

Figure S14. Raman spectrum of Mn_3O_4@rGO hybrid aerogels. The value of I_D/I_G in Mn_3O_4@rGO hybrid aerogels (1.56) is similar to that in rGO aerogels (1.51), indicating that the surface energy-driven strategy is a nondestructive approach introducing few, if any, defects to the rGO.

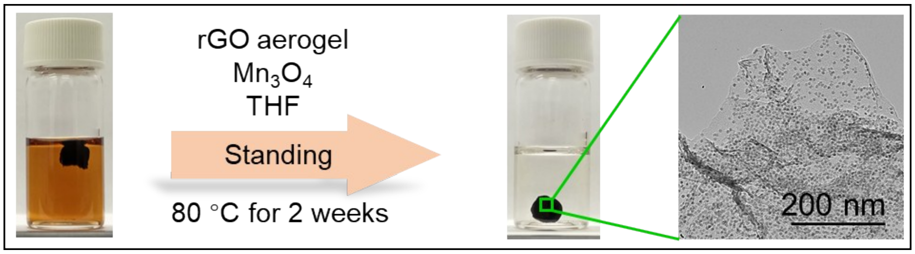

Figure S15. Digital photographs of the assembly process at 80 °C and the corresponding TEM image of the resulting Mn_3O_4@rGO hybrid aerogels. Obviously, the assembly time is only reduced to two weeks, indicating that the assembly process is hardly influenced by the Brownian motion.

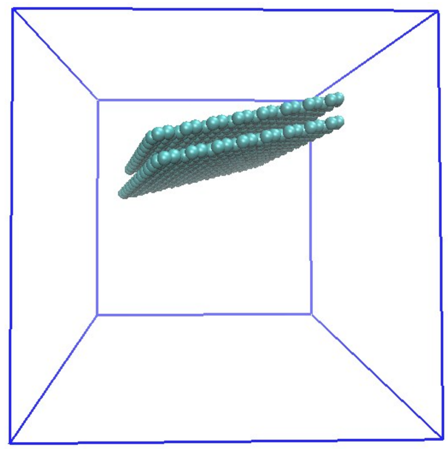

Figure S16. Final state of two graphene nanosheets in THF. For clarity, the THF molecules are not shown.

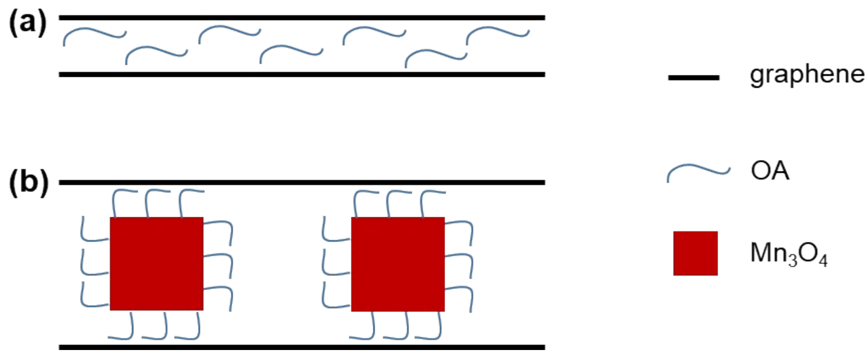

Figure S17. The microscopic view in the dispersion of two graphene nanosheets with the help of OA molecules and (b) OA-modified Mn_3O_4 nanocubes. As shown in panel (a), at a microscopic level a lot of OA molecules are needed in the dispersion of two graphene sheets. In contrast to the soft surfactants, only several grafted nanoparticles are needed to keep the graphene sheets apart, as shown in panel (b).

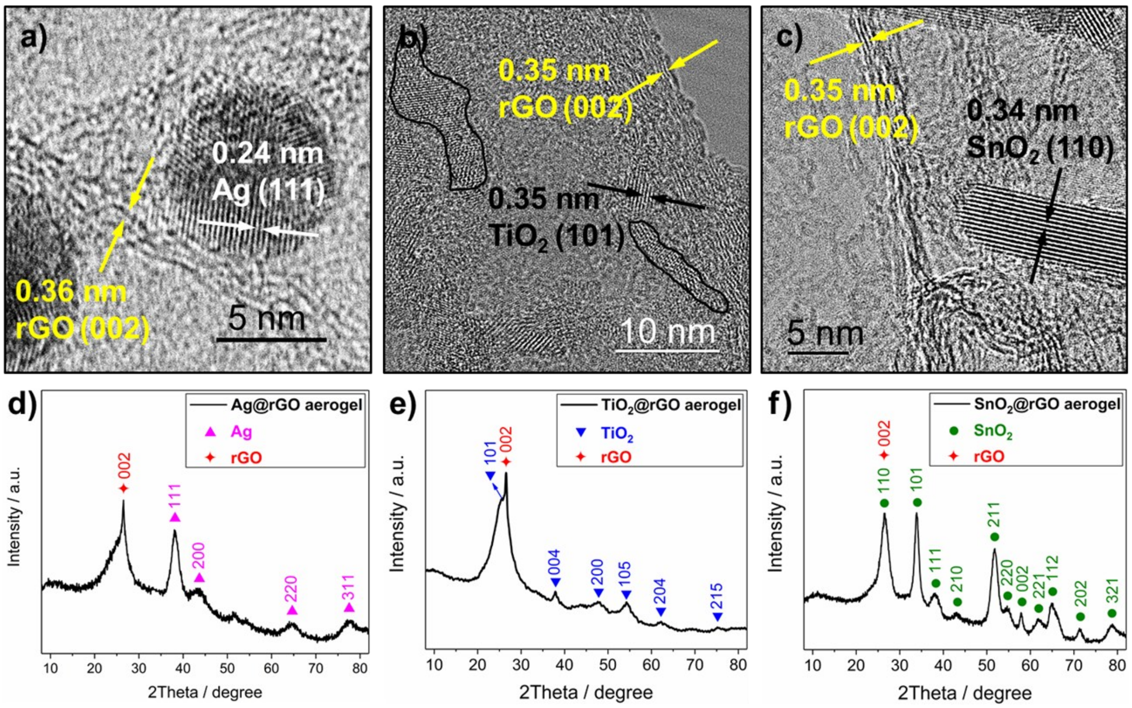

Figure S18. (a), (b) and (c) HRTEM images, and (d), (e) and (f) XRD patterns of Ag@rGO, TiO_2@rGO and SnO_2@rGO hybrid aerogels, respectively.

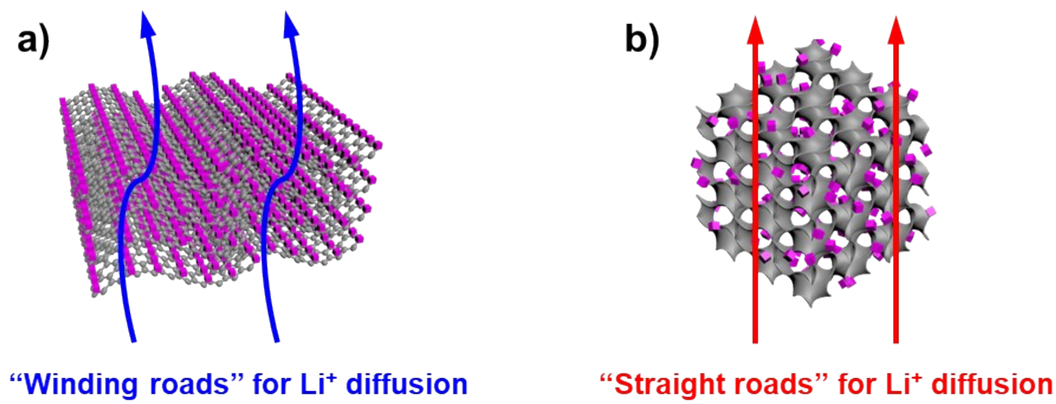

Figure S19. Schematic illustration of the Li^+ diffusion pathways in (a) Mn_3O_4@rGO nanocomposites and (b) Mn_3O_4@rGO hybrid aerogels.

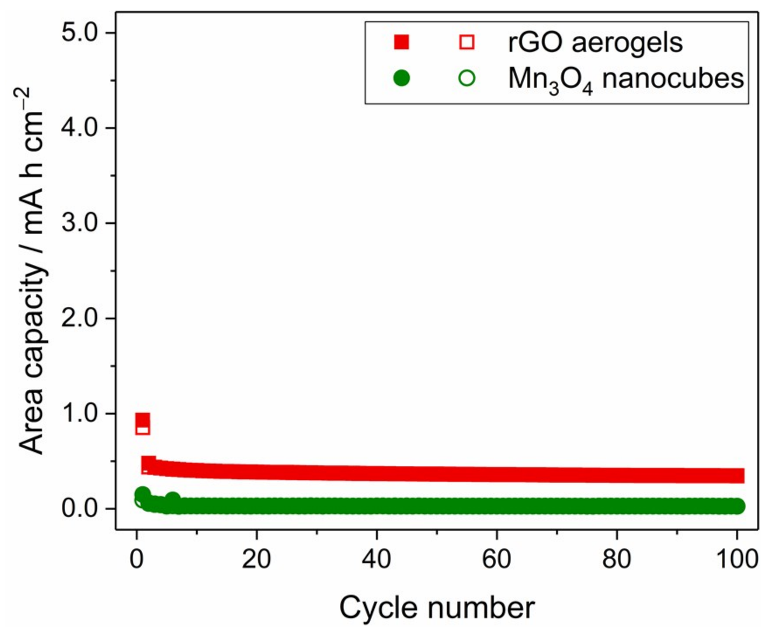

Figure S20. Cycling behavior of pure Mn_3O_4 nanocubes and pure rGO aerogels at a mass loading density of 7 mg cm^{-2} (current density = 3.5 mA cm^{-2}).

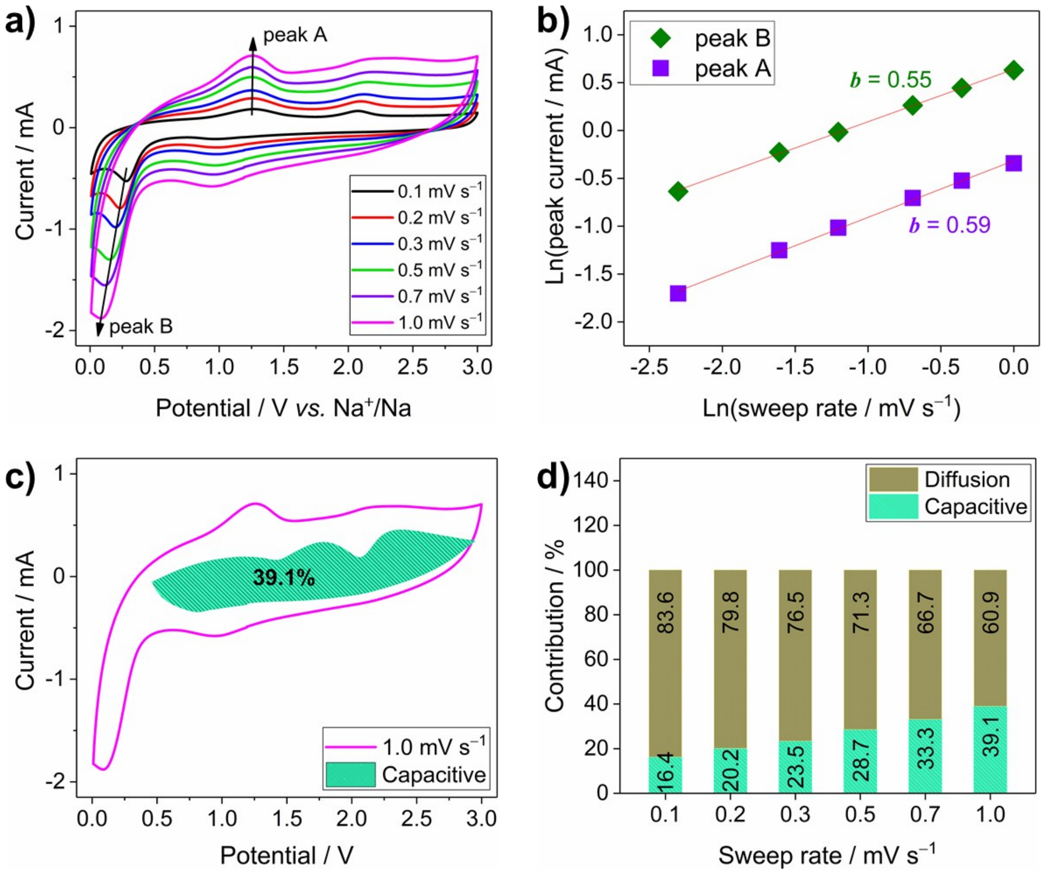

Figure S21. (a) CV curves of the Mn_3O_4@rGO hybrid aerogels at different sweep rates (0.1–1 mV s^{-1}); (b) relationship between peak current and sweep rate (plotted with natural logarithm axis); (c) CV curve with corresponding capacitive contribution (shadow) at 1 mV s^{-1}; (d) capacitive contribution ratios at different sweep rates. The capacitive contribution is calculated in the voltage range of 0.45–3.0 V, because the polarization effect below 0.45 V is strong.

References

[S1] J. Gao, M. A. Lowe, H. D. Abruña, *Chem*. *Mater*. 2011, 23, 3223.

[S2] L. Pan, X. D. Zhu, X. M. Xie, Y. T. Liu, *J. Mater. Chem. A* **2015**, *3*, 2726.

[S3] F. J. Heiligtag, M. D. Rossell, M. J. Süess, M. Niederberger, *J. Mater*. *Chem*. **2011**, *21*, 16893.

[S4] L. Pan, K. X. Wang, X. D. Zhu, X. M. Xie, Y. T. Liu, *J. Mater. Chem. A* **2015**, *3*, 6477.

[S5] H. Hu, Z. Zhao, W. Wan, Y. Gogotsi, J. Qiu, *Adv. Mater.* **2013**, *25*, 2219.

[S6] S. Stankovich, D. A. Dikin, R. D. Piner, K. A. Kohlhaas, A. Kleinhammes, Y. Jia, Y. Wu, S. T. Nguyen, R. S. Ruoff, *Carbon* **2007**, *45*, 1558.

[S7] Y. T. Liu, Q. P. Feng, X. M. Xie, X. Y. Ye, *Carbon* **2011**, *49*, 3371.